Title page

Effect of colloidal particle size on physicochemical properties and aggregation behaviors of two alkaline soils

Yu-yang Yan[1], Xin-ran Zhang[1], Chen-yang Xu[1,2]*, Jun-jun Liu[1], Fei-nan Hu[3,4], Zeng-chao Geng[1,2]

(1. *College of Natural Resources and Environment*, *Northwest A&F University*, *Yangling*, *Shaanxi* 712100, *China*; 2. *Key Laboratory of Plant Nutrition and the Agri-environment in Northwest China, Ministry of Agriculture, Northwest A&F University, Yangling, Shaanxi 712100, China; 3. State Key Laboratory of Soil Erosion and Dryland Farming on the Loess Plateau, Northwest A&F University, Yangling, Shaanxi 712100, China; 4. Institute of Soil and Water Conservation, Chinese Academy of Sciences, Ministry of Water Resources, Yangling, Shaanxi 712100, China*)

***Corresponding author:**

Chen-yang Xu

Email address: xuchenyang@nwafu.edu.cn, xuchenyang.ms@163.com;

Postal address: College of Natural Resources and Environment, Northwest A&F University, No. 3 Taicheng Road, Yangling District, Shaanxi 712100, China.

Abstract

Soil cColloidal particles are the most most active soil components of all, and they also vary in elemental composition and environmental behaviors with the particle size due to the heterogenous nature of natural soils. The purposes of the present study are to clarify how particle size affects the physiochemical properties and aggregation kinetics of soil colloids, and to further reveal the underlying mechanisms. Soil colloidal fractions,particles from two alkaline soils—Lou soilAnthrosol and cinnamon soilCalcisol were subdivided into three ranges: $d < 2$ μm, $d < 1$ μm and $d < 100$ nm. The organic and inorganic carbon contents, clay mineralogy, surface electrochemical properties, including surface functional groups and zeta potentials, were characterized. Through time-resolved light scattering technique, the aggregation kinetics of soil colloidal fractions were investigated, and their critical coagulation concentrations (CCCs) were determined. With decreasing colloidal particle diameter, the total carbon content, organic carbon, organic functional groups content and illite content all increased. The absolute zeta potential became values less negative and the charge variability decreased with decreasing particle diameter. The CCC values of Lou soilAnthrosol and cinnamon soilCalcisol colloids followed the descending order of $d <$ 100 nm, $d < 1$ μm, $d < 2$ μm. Compared with the course factions ($d < 1$ μm and $d < 2$ μm), soil nanoparticles were more abundant in organic carbon and more stable clay minerals ($d < 100$ nm), thus they exhibited strongest colloidal suspension stability. The differences in organic matter contents and clay mineralogy are the fundamental reasons for the differences in colloidal suspension stability behind the size effects of Lou

~~soil~~Anthrosol and ~~cinnamon soil~~Calcisol colloids. The present study revealed the size effects of two alkaline soil colloids on carbon content, clay minerals, surface properties and suspension stability, emphasizing that soil nanoparticles are prone to be more stably dispersed instead of being aggregated. These findings can provide references for in-depth understanding of the environmental behaviors of the heterogeneous soil organic-mineral complexes.

Keywords: Nanoparticles; Clay mineral composition; zeta potential; Critical coagulation concentration

1. Introduction

Soils contain a series of solid particles in continuous sizes, ranging over six orders of magnitude from nanometers to millimeters (Lead and Wilkinson, 2006; Li et al., 2011), among which soil colloids are the most reactive fractions. ~~active parts.~~ Soil colloids are characterized by high surface area and abundant surface charges, exhibiting high potential for carbon sequestration and strong adsorption capacity~~Soil colloids are characterized by high surface area and strong adsorption capacity~~, which can largely determine the fate and transport of pathogens, nutrients, heavy metals and organic pollutants, and might cause environmental problems to adjacent water bodies or groundwater (Baalousha et al., 2009; Calabi-Floody et al., 2011). Due to their high reactivity and fluidity in aqueous environment, soil colloids play an important role in physical, chemical and biogeochemical processes ~~of~~ in natural environment (Schäfer et al., 2012; Mayordomo et al., 2016). The capacity of soil colloids in mobilizing bound ~~driving attached~~ nutrients and pollutants is closely related to their dispersion stability under various environmental conditions (Won and Burns, 2018). Therefore, studies on the dispersion stability of soil colloids have attracted extensive attention.

Currently, the definition of soil and environmental colloidal fractions is ambiguous. Soil colloidal fractions are defined as soil particles in diameter of < 1 μm (Lead and Wilkinson, 2006; Weil and Brady, 2016), and also being of < 2 μm (Zhang et al., 2021); while in some extreme cases, they can refer to the particles in diameter of 5–10 μm (Yin et al., 2010). Such discrepancies are seen among publications due to the fact that colloids are defined based on the particle diameter range within which they can display

colloidal properties. Since for different materials, e.g., metal (Fe/Al/Ti) oxides, silica gel, phyllosilicates, the specific colloidal range differs greatly.

Compared with engineered nanoparticles with known mineralogical organization, natural soils are much more heterogeneous (Cárdenas et al., 2010); their elemental composition and clay mineralogy of soil colloids change with particle size. Tsao et al., (2013) found that quartz and feldspar were mainly dominant in colloidal particles of < 2 μm and 450–2000 nm in red soil (Ferralsols, WRB, IUSS Working Group WRB. 2022), while illite and montmorillonite were the main clay minerals in nanoparticles (1–100 nm). In addition, the mineral structure at nanometer scale also changes. Compared with colloidal particles of < 2 μm, the Si/Al ratio in nanoparticles increased, and the surface area, morphology, crystallinity, surface atomic structure and frame structure were significantly different (Tsao et al., 2011). Furthermore, particle size also affects the surface potential of soil colloids. Tang et al., (2015) investigated the surface potential variations with particle size (1–10 μm, 0.5–1 μm, 0.2–0.5 μm, < 0.2 μm) for variably-charged yellow soil (Lixisols) and permanently-charged purple soil (Leptosols); among the colloidal fractions, the absolute surface potential of the finest particles of purple soil (Leptosols) was lowest while that of the yellow soil (Lixisols) was the largest, caused by the differences in surface charge density. Thus, the influences of particle size on elemental composition and surface properties of soils should be further studied.

In recent years, great progress has been made in the study of dispersion stability of soil clay minerals, such as montmorillonite, kaolinite, illite or hematite, and soil

nanoparticles (Xu et al., 2018; Sun et al., 2020; Wei et al., 2021; Zhu et al., 2014). He et al., (2008) demonstrated that hematite nanoparticles with various particle diameters showed different surface properties and aggregation behaviors under the same pH conditions; moreover, the critical coagulation concentrations (CCCs) of hematite decreased with the decrease of particle diameter. Zhou et al., (2013) compared the CCCs of ten different TiO_2 nanoparticles with varying sizes and indicated that crystal structure and particle diameter both affected the aggregation behaviors of TiO_2. Zhang et al. (2016) confirmed that the types of clay minerals for two Alfisols changed from smectite and vermiculite to kaolinite and illite when the particle size varied from colloids to nanoparticles. Therefore, the dependence of physiochemical properties, surface properties and environmental behaviors on particle size for heterogeneous soil colloidal particles needs systematic investigation.

In the present study, soil colloidal particles of two alkaline soils—~~Lou soil~~Anthrosol and ~~cinnamon soil~~Calcisol were subdivided into three ranges: $d < 2$ μm, $d < 1$ μm and $d < 100$ nm. Their organic fraction and clay mineralogy, surface electrochemical properties and colloidal stability were studied. This study selected two representative calcareous soils to verify the following scientific hypothesis: soil colloids are organic-inorganic composites. As particle diameter decreases (from colloid particles to nanoparticles), the number of organic functional groups on the surface of soil colloids increases, and the type of clay minerals shifts towards finer clay particles, e.g. illite, resulting in increased specific surface area and decreased charge density, and thus enhanced suspension stability, meaning particle diameter influences the

composition of soil colloidal fractions, thereby changing surface properties and suspension stability. The findings can have important implications for predicting the environmental performances of colloids and colloid-facilitated nutrients, pollutes and pathogens in natural soil and water environment.

~~The objectives of the present study are to clarify how particle size affects the surface properties and aggregation behaviors of soil colloids, and to analyze the underlying mechanisms. The findings are of important significances for predicting the environmental performances of colloids and colloid-facilitated nutrients, pollutes and pathogens in natural soil and water environment.~~

2. Materials and methods

2.1 Soil sampling

The study collected two surface soil samples (0–20 cm), Lou soil and Cinnamon soil, being calcareous soils, by mixing soils form 5–10 sampling points using a stainless-steel auger at Yangling District (N38°18′14″ and E108°2′30″), and Zhouzhi Country (N34°8′8″ and E108°3′10″), in Shaanxi province, northwest China, respectively. According to World Reference Base for Soil Resources (WRB, IUSS Working Group WRB. 2022), the Lou soil and Cinnamon soil are classified as Calcic Protocalcic Calcisols (Loamic, Lixic, Humic) and Hortic Endoanthric Anthrosols (Loamic, Luvic, Eutric, Calcic), respectively. Both types of soil developed from loess parent material. The typical soil profile configuration for the tested Anthrosol is Ap1-Ap2-Bt-Bk-C, while for the Calcisol, it is Ah-Bt-Bk-C.

Soils samples were taken back to laboratory for air-drying and sieving. The basic

soil properties were determined based on standard methods. Soil pH was measured with a pH electrode, employing a solution-to-soil ratio of 2.5:1. Soil organic carbon (SOC) was determined using the $K_2Cr_2O_7$ oxidation method. The cation exchange capacity (CEC) of soil was measured with exchange method. The $CaCO_3$ content was determined by gasometric method. The free Fe/Al oxides were extracted by dithionite-citrate-bicarbonate (DCB) solution. The particle size distribution was measured using the laser diffractometer of Malvern Mastersizer 2000 (Malvern Instruments Ltd., UK). The pH of Anthrosol was 8.34 while it was 8.32 for the Calcisol. The SOC of Anthrosol and Calcisol were 7.25 $g \cdot kg^{-1}$ and 9.22 $g \cdot kg^{-1}$, respectively. The CEC of Anthrosol and Calcisol were 25.9 $cmol \cdot kg^{-1}$ and 22.2 $cmol \cdot kg^{-1}$.The contents of $CaCO_3$ in Anthrosol and Calcisol were 51.7 $g \cdot kg^{-1}$ and 82.5 $g \cdot kg^{-1}$. The Free Fe/Al oxides content of Anthrosol and Calcisol were 22.8 $g \cdot kg^{-1}$ and 23.1 $g \cdot kg^{-1}$. The proportions of Sand (2–0.02 mm), Silt (0.02–0.002 mm) and Clay (<0.002 mm) in Anthrosol were 34.0%, 40.6% and 25.4% while those were 28.0%, 44.8% and 27.2% for the Calcisol.

~~Two representative surface soils (0–20 cm) were collected from the Guanzhong Plain, China, namely Lou soil (agricultural soil) and cinnamon soil (natural soil). Lou soil was collected from Yangling District, Shaanxi Province. Cinnamon soil was collected from Zhouzhi County, Shaanxi Province. Lou soil and cinnamon soil are classified as Anthrosols and Calcisols, respectively, according to the FAO soil classification. Soils were taken back to laboratory for air-drying and sieving. The basic soil properties are determined based on standard methods. The pH of Lou soil was 8.34 while it was 8.32 for the cinnamon soil. The organic carbon contents of Lou soil and~~

~~cinnamon soil were 7.25 g·kg^{-1} and 9.22 g·kg^{-1}, respectively. The contents of $CaCO_3$ in Lou soil and cinnamon soil were 51.7 g·kg^{-1} and 82.5 g·kg^{-1}. The Free Fe/Al oxides content of Lou soil and cinnamon soil were 22.8 g·kg^{-1} and 23.1 g·kg^{-1}.~~

2.2 Extraction of soil colloidal fractions in different size ranges

The soil colloidal particles were extracted based on the Stokes' law, and the detailed procedures can be found in our previous publication (Hu et al., 2022). Briefly, 50 g of dry soil was weighed into a beaker containing 500 mL of distilled water~~weigh 50 g soil into a beaker containing 500 mL distilled water~~, and put the suspension under sonication for an hour using the ultrasonic cell disrupter (XO-900D, Nanjing Xianou Instruments Corporation, China) while maintaining the temperature below 30°C. Afterwards, the suspension was transferred to a larger beaker and distilled water was added to make up the total volume of 5 L. The suspension was further dispersed using an electronic blade stirrer (JB-200, Shanghai Nanhui Huiming Apparatus, China) for one hour, before being sieved~~sifted~~ through ~~a 300-mesh~~ sieve with a pore size of 53 μm, and the upper suspensions containing soil colloidal particles in different diameters were collected by centrifugation. Based on the equation (1), centrifugation speed and time for colloidal particles of d < 2 μm, < 1 μm and < 100 nm ~~are~~ were calculated and shown in Table S1.

$$t = \frac{\eta \lg \frac{R_2}{R_1}}{3.81 N^2 r^2 \Delta d} \quad (1)$$

in which, t is time for centrifugation (s); R_1 is the distance from the surface of the liquid to the center of the axis of the centrifuge, here is 5.7 cm; R_2 is distance from the particles

to the center of the axis of the centrifuge, here is 10.5 cm; N (rev·s^{-1}) is the centrifuge speed; r (cm) is the desired colloidal particle radius; Δd is the difference in density between the soil particles (2.65 g·cm^{-3}) and water (1 g·cm^{-3}), while Δd is 1.65 g·cm^{-3}; η is the water viscosity coefficient, here is 0.00839 g·cm^{-1}·s^{-1} at 25 °C.

2.3 Characterization of soil colloidal fractions in different size ranges

The initial particle diameters of soil colloids were determined by a time-resolved dynamic light scattering (DLS) apparatus (Nanobrook Omni, Brookhaven, USA). The organic carbon contents in soil colloids were determined by potassium dichromate external heating method and total carbon content was determined by elemental analyzer (Elementar Vario EL III, Germany). The inorganic carbon content was calculated by subtraction method (Wang et al., 2011). The clay mineralogy of soil colloids was determined by the XRD (Ultima-IV, Rigaku, Japan), and by comparing the intensity of the dominant X-ray diffraction peak of the soil mineral colloid to a standard mineral reference (Database ICDD 2004), the relative percentage content of the minerals was determined. The specific surface areas of the soil colloids were measured by BET-N_2 method (ASAP 2460, Micromeritics instrument, USA). High-resolution spectra of C1s and O1s of soil colloids were acquired by X-ray photoelectron spectroscopy (XPS) (Thermo Scientific K-Alpha, USA) (Luo et al., 2019), and the Gaussian−Lorentzian curve-fitting program (XPSPEAK 4.1) was used to analyze the XPS spectra ~~(Luo et al., 2019)~~. The zeta potentials of soil colloids were measured by Zeta PALS equipped with a BI-ZTU Autotitrator (ZetaPALS, Brookhaven, USA) with 1 mmol·L^{-1} NaCl solution as the background electrolyte; and the pH range of colloidal suspension was set to 3–

10 adjusted with 0.1 mol·L^{-1} HCl and NaOH. The concentrations of K^+, Na^+, Ca^{2+}, and Mg^{2+} in soil colloidal suspensions were measured by flame atomic absorption spectrophotometry (PinAAciie 900F, USA).

2.4 Aggregation kinetics of soil colloidal fractions

The aggregation kinetic curves of soil colloidal particles in different electrolytes were determined by time-resolved DLS measurements. The incident wavelength was 635 nm and the scattering angle was 90°. ~~While using the DLS instrument, it is necessary to clean up the surrounding dust, especially the sample pool.~~ The stock colloidal suspensions with particle concentration of 200 mg·L^{-1} were mixed with electrolyte solutions with equal volume. The suspension pH was adjusted to 8.0, which was close to the pH value of natural soil with addition of 0.1 mol·L^{-1} HCl or NaOH before measurement. The chosen electrolyte concentrations for NaCl and $CaCl_2$ were 200–2000 and 2–20 mmol·L^{-1}. The effective diameter (D_h) of the mixed sample was automatically recorded every 2 min, and an aggregation kinetic curve was obtained in 30 min monitoring.

2.5 Calculation of critical coagulation concentration

According to the particle interaction theory, the aggregation kinetic curves under electrolyte conditions can be divided into reaction-limited aggregation (RLA) stage under low concentration which was affected by electrolyte conditions and diffusion-limited aggregation (DLA) stage under high concentration which was not affected by electrolyte concentration. The CCC is the critical electrolyte concentration when the aggregation process changes from the RLA state ($\alpha < 1$) to the DLA state ($\alpha = 1$).

Attachment efficiency (α) represents the bonding probability of particle collisions and can be calculated for each electrolyte concentration by using equation 2, which allowed the curve of α as a function of electrolyte concentration to be plotted (Xu et al., 2020a; Hu et al., 2022).

$$\alpha_{\exp} = \frac{1}{W} = \frac{k_{11}}{(k_{11})_{fast}} = \frac{\frac{1}{N_0}\left(\frac{da_h(t)}{dt}\right)_{t\to 0}}{\frac{1}{(N_0)_{fast}}\left(\frac{da_h(t)}{d_t}\right)_{t\to 0,\, fast}} \quad (2)$$

where D_h is the effective diameter of particles, t is the time (min); N_0 is the density of particles; K_{11} is the aggregation rate of RLA; $(K_{11})_{fast}$ is the aggregation rate of DLA. The intersection of RLA regime and DLA regime is the CCC.

The aggregation rates were calculated by the average of the last 5 effective diameters divided by the aggregation time at specific electrolyte concentration. The fractal dimension in the DLA regime was obtained based on the method proposed by Wang et al. (2013).

$$D(t) = b * t^n + D_0 \quad (3)$$

in which, $D(t)$ is the colloidal effective diameter at time t (min), D_0 is the initial effective diameter of colloids, and b and n are constants determined by the aggregation curves. The fractal dimension is $d_f = 1/n$ in the DLA regime.

3. Results and discussion

3.1 Particle size and distribution characteristics of ~~Lou soil~~Anthrosol and ~~cinnamon soil~~Calcisol colloidal fractions

The average diameters of ~~Lou soil~~Anthrosol and ~~cinnamon soil~~Calcisol colloids

were measured by time-resolved DLS, and the results were shown in Table 1. The number-weighted diameters for Anthrosol colloids of d < 2 μm were about 1.04 times of d < 1 μm, and about 1.84 times of d < 100 nm, respectively. The intensity-weighted diameters for Anthrosol colloids were 294.10~396.81 nm. For Calcisol colloidal fractions, the number-weighted diameters for colloids of d < 2 μm were about 1.07 times of d < 1 μm, and about 1.65 times of d < 100 nm, and the intensity-weighted diameters were 312.25~439.20 nm. ~~The number-weighted diameters for Lou soil colloids of d < 2 μm, < 1 μm and < 100 nm were 133.16, 127.84 nm and 72.47 nm, respectively. The intensity-weighted diameters were 396.81 nm, 371.45 nm and 294.10 nm. For cinnamon soil colloidal fractions, the number-weighted diameters for colloids of d < 2 μm, < 1 μm and < 100 nm were 141.23 nm, 131.67nm and 85.48 nm, and their intensity-weighted diameters were 439.20 nm, 372.07nm and 312.25 nm, respectively.~~ The intensity-weighted diameters were generally higher than the number-weighted diameters, especially in polydisperse system (Xu et al., 2020b). ~~The particles in the soil solution are in constant Brownian motion, and when light passes through the colloids, the particles will undergo light scattering, resulting in fluctuations in light intensity, and thus the effective diameter (intensity-weighted diameter) of the particles is calculated (Filella et al., 1997).~~ The colloidal particles in the soil solution were in constant Brownian motion, upon illumination by light, these colloidal particles scatter light, causing variations in light intensity. This phenomenon allowed for the calculation of the effective diameter of the particles, which was the intensity-weighted diameter (Filella et al., 1997). Given that particle diameter is proportional to the sixth power of

light intensity. Consequently, in polydisperse systems where larger particles were present, the number-weighted diameter provided typically a more accurate representation of the true diameter of colloidal particles (Xu et al., 2015).~~Since the particle diameter is proportional to the sixth power of the light intensity, that is, if there are larger particles in the solution in such polydisperse systems, the number-weighted diameter is generally more representative of the true diameter of colloidal particles (Xu et al., 2015).~~

(*Insert Table 1 near here*)

From table 1, it can be seen that the average colloidal diameters of $d < 2$ μm were close to that of $d < 1$ μm, and they were both significantly higher than that of the nano-sized fraction. From the particle size distribution characteristics, it is clear that the size range indicated by the differences of D_{90} and D_{10} increased with intended particle diameter. For ~~Lou soil~~Anthrosol and ~~cinnamon soil~~Calcisol, 74.69% and 63.55% of all particles contained in the colloidal suspensions of $d < 100$ nm were actually less than 100 nm, respectively, indicating the complexity of soil colloidal particle irregularity.

3.2 Physiochemical properties and clay mineralogy of ~~Lou soil~~Anthrosol and ~~cinnamon soil~~Calcisol colloids

Table 2 shows the physiochemical properties of soil colloidal fractions. The yields of each colloidal fraction of ~~Lou soil~~Anthrosol were slightly larger than that of ~~cinnamon soil~~Calcisol, respectively. The yields of colloidal particles of $d < 2$ μm were about 1.3~1.4 times of $d < 1$ μm, and about 4.0~4.9 times of $d < 100$ nm, respectively. With the decreasing colloidal particle diameter, the total carbon content, organic carbon

and inorganic carbon content all increased, suggesting the finer particles were richer in carbon. This tendency is in agreement with other publications (Zhang et al., 2021; Said-Pullicino et al., 2021; Hu et al., 2022). The specific surface areas for colloidal fractions of $d < 1$ μm were largest of all, which may be related to the structures of formed clusters while drying the samples for observation under microscopy (Yu et al., 2017; Weissenberger et al., 2021). Furthermore, Anthrosol and Calcisol nanoparticles exhibited the lowest specific surface area. This phenomenon raised from Organic substances adsorb relatively little inorganic nitrogen (Li et al., 2013; Wilson et al., 2008). Therefore, However, to our knowledge, no other better method has been reported for measuring the specific surface area of natural nanoparticles.

(*Insert Table 2 near here*)

The clay mineralogy of ~~Lou soil~~Anthrosol and Calcisol~~cinnamon~~ colloidal fractions is shown in Table 3. ~~Cinnamon soil~~Calcisol colloidal fractions were dominant by illite, kaolinite and chlorite while there was less chlorite in ~~Lou soil~~Anthrosol colloidal fractions. With the decrease of particle size, the content of illite increased and kaolinite content decreased. This tendency is in agreement with other publications (Chenu and Plante, 2006; Zhang et al., 2016). Among the dominant clay types, the size of illite is finer than kaolinite and chlorite (Weil and Brady, 2016), so its mass percentage was higher in the nano-sized fraction.

(*Insert Table 3 near here*)

3.3 Surface properties of ~~Lou soil~~Anthrosol and ~~cinnamon soil~~Calcisol colloids

The XPS spectra of soil colloidal fractions are shown in Fig. 1. From Fig. 1, it can

311 be seen that the main C-containing functional groups were C–C/C-H/C=C, C–O, C=O,
312 and COO- groups at 284.6, 286.2, 288.0 and 289.4 eV, respectively (Liang et al., 2020;
313 Ding et al., 2023). The functional groups for colloidal particles of d < 100 nm were
314 more abundant than those for colloids of d < 2 μm and d < 1 μm, while there were no
315 significant differences between colloids of d < 2 μm and d < 1 μm. With the decrease
316 of colloidal particle diameter, the relative contents of oxygen-containing functional
317 groups (C–O, C=O, COO-) gradually decreased. Specifically, the content decreased
318 gradually from 32.01% in Lou colloids of d < 2 μm to 20.93% in Lou colloids of d <
319 100 nm (Table S2). The functional groups of C–O and COO- gradually decreased until
320 they eventually disappeared, more C=O groups were exposed to the surrounding air.
321 For ~~cinnamon soil~~Calcisol colloids (Fig. 1d, e, f), the relative contents of organic
322 oxygen-containing functional groups for colloidal particles of d < 2 μm, d < 1 μm and
323 d < 100 nm showed a different trend, compared with that in ~~Lou soil~~Anthrosol colloids.
324 The relative contents of organic oxygen-containing functional groups gradually
325 increased with the decrease of diameter. This trend was particularly pronounced in
326 fraction of d < 100 nm, and contents of C–O and COO- were highly increased (Table
327 S2).

328 (*Insert Figure 1 near here*)

329 Oxygen-containing functional groups of C–O, C=O and COO- are electronegative
330 functional groups, hydroxyl and carboxyl groups can lose protons and make the surface
331 of soil colloidal particles carry negative charges (Audette et al., 2021). Functional
332 groups of C–O, C=O and COO- can affect the negative charges carried on the colloidal
333 surface by forming hydrogen bonds, and their polarity can also affect the negative
334 charges on the surface when O atom combines with C and H. The electrons will lean

towards the O atom with stronger electronegativity, which also makes the colloidal surface carry negative charges (Tan et al., 2019). The contents and types of oxygen-containing functional groups are one of the main factors affecting colloid charge and aggregation.

The zeta potential values of different colloidal fractions at the pH range of 3–10 are shown in Fig. 2. Zeta potentials of the colloidal particles were negative, indicating that they were negatively-charged. The ~~absolute values of~~ zeta potentials ~~for~~of ~~of Lou soil~~Anthrosol and ~~cinnamon soil~~Calcisol colloidal particles ~~increased~~were more negative with increasing solution pH, due to the deprotonation of the surface (Moayedi and Kazemian, 2013; Dong et al., 2019). Compared with the ~~cinnamon soil~~Calcisol colloids, the zeta potentials of ~~Lou soil~~Anthrosol colloidal particles were more negative, due to Anthrosol possessed a higher surface charge density. For ~~cinnamon soil~~Calcisol colloids, the differences among colloidal fractions were larger.

(*Insert Figure 2 near here*)

In general, ~~the absolute~~ zeta potential became more negative with increasing particle diameter. ~~values increased with increasing particle diameter.~~ When the pH changed from 3 to 10, for every pH unit increased, the zeta potential values of ~~Lou soil~~Anthrosol colloids of d < 2 μm, < 1 μm, and < 100 nm would be increased by 2.14 mV, 2.09 mV and 1.89 mV; and for ~~cinnamon soil~~Calcisol colloids, those variation rates were 2.15 mV, 1.45 mV and 1.37 mV, respectively. Those data demonstrate that the charge variability decreasing with the decreasing particle diameter. Song et al., (2019) compared the zeta potential of wheat straw biochar nanoparticles (< 100 nm) and

colloidal particles (< 1000 nm), and found that the absolute values of colloidal particles were larger at same pH, which was explained by the differences in the number of surface carboxyl and hydroxyl groups. The zeta potential of colloidal particles is proportional to charge density, which means that it is related to both charge quantity and specific surface area (Hou et al., 2009). Therefore, the size effect of zeta potential of ~~Lou soil~~Anthrosol and ~~cinnamon soil~~Calcisol colloidal particles is mainly related to the reduction of charge density caused by larger specific surface area of nanoparticles (Xu et al. 2020b).

3.4 Aggregation kinetics curves of ~~Lou soil~~Anthrosol and ~~cinnamon soil~~Calcisol colloids in NaCl and $CaCl_2$ solutions

The aggregation kinetics of ~~Lou soil~~Anthrosol and ~~cinnamon soil~~Calcisol colloids in NaCl and $CaCl_2$ solutions are shown in Figs. S1 and S2. The aggregation process of soil colloids was divided into RLA and DLA stages. The RLA stages for ~~Lou soil~~Anthrosol colloids of d < 2 μm, d < 1 μm and d < 100 nm in NaCl solution were 0–80, 0–80 and 0–100 mmol·L^{-1}, respectively, during which repulsive forces existed between the particles and attachment did not occur on every collision. As the electrolyte concentration continued to increase, the solution entered into the DLA regime. At this point, attachment occurred with every collision between particles, and the aggregation rates were not affected by the electrolyte concentration. At last, the effective diameters of the formed clusters were stable at around 1600 nm. Figure S1b, d and f showed that the aggregation behaviors of ~~Lou soil~~Anthrosol colloids in $CaCl_2$ solution were similar to that in NaCl solution, and the corresponding $CaCl_2$ concentrations for ~~Lou~~

~~soil~~Anthrosol colloids of $d < 2$ μm, $d < 1$ μm and $d < 100$ nm in RLA stage were about 0–1.5, 0–1.5 and 0–2 mmol·L^{-1}, respectively.

The aggregation kinetics of ~~cinnamon soil~~Calcisol colloids in NaCl and $CaCl_2$ solutions were similar to ~~Lou soil~~Anthrosol colloids (Fig. S2). The RLA stages for ~~cinnamon soil~~Calcisol colloids of $d < 2$ μm, $d < 1$ μm and $d < 100$ nm in NaCl solution were 0–100, 0–120 and 0–250 mmol·L^{-1}, and were about 0–1.8, ~~,~~ 0–1.7 and 0–2 mmol·L^{-1} in $CaCl_2$ solution, respectively. The effective diameters of the clusters for ~~cinnamon soil~~Calcisol colloids were stabilized at about 1600 nm and 1800 nm in NaCl and $CaCl_2$ solutions, respectively.

Aggregation rates of soil colloids varied with particle diameters at the same electrolyte concentration, which was particularly evident in RLA stage (Table 4). With decreasing particle diameter, the aggregation rates of Anthrosol and Calcisol colloids in 50 mmol·L^{-1} NaCl and 1 mmol·L^{-1} $CaCl_2$ solutions exhibited a corresponding decline. In addition, in 50 mmol·L^{-1} NaCl solution, the aggregation rates for Anthrosol colloids of $d < 2$ μm, $d < 1$ μm and $d < 100$ nm were about 2.17, 2.09 and 1.95 times those of Calcisol colloids, while the aggregation rates were about 1.46, 1.57 and 1.91 times those of Calcisol colloids in 1 mmol·L^{-1} $CaCl_2$ solution, respectively. ~~For Lou soil colloids of $d < 2$ μm, $d < 1$ μm and $d < 100$ nm with addition of 50 mmol·L^{-1} NaCl, aggregation rates were 19.46, 14.91 and 7.22 nm·min^{-1}, respectively, while those of cinnamon soil colloids were 8.98, 7.15 and 3.95 nm·min^{-1} with decreasing particle diameter. In 1 mmol·L^{-1} $CaCl_2$ solution, the aggregation rates of cinnamon soil colloids of $d < 2$ μm, $d < 1$ μm and $d < 100$ nm were 8.22, 7.33 and 5.22 nm·min^{-1}, respectively.~~

Therefore, from table 4, the aggregation rates of ~~Lou soil~~Anthrosol and ~~cinnamon soil~~Calcisol colloids showed the size effect. From table 4, it could be observed that the fractal dimensions in NaCl solutions were largely higher than those in $CaCl_2$ solutions, suggesting a much denser structure (Meng et al., 2013). In other words, the formed structures in divalent solutions were more open.

(*Insert Table 4 near here*)

3.5 Suspension stability of ~~Lou soil~~Anthrosol and ~~cinnamon soil~~Calcisol colloids in NaCl and $CaCl_2$ solutions

The CCCs for ~~Lou soil~~Anthrosol colloids of $d < 2$ μm, $d < 1$ μm and $d < 100$ nm in NaCl solution were 80.40, 91.78 and 134.96 mmol·L^{-1}, respectively (Fig. 3a), and those for ~~cinnamon soil~~Calcisol colloids were 121.10, 126.50 and 292.86 mmol·L^{-1}, respectively (Fig. 3b). The CCCs increased with the decreasing particle diameter, indicating that the suspension stability of soil nanoparticles was stronger than those of colloidal particles.

(*Insert Figure 3 near here*)

In $CaCl_2$ solutions, the CCCs for ~~Lou soil~~Anthrosol colloids of $d < 2$ μm, $d < 1$ μm and $d < 100$ nm were 1.61, 1.68 and 1.77 mmol·L^{-1}, respectively, and for ~~cinnamon soil~~Calcisol colloids, those corresponding values were 1.90, 1.91 and 2.13 mmol·L^{-1} (Fig. 4). The CCCs in $CaCl_2$ solutions also increased with the decreasing particle size. The contents of K^+, Na^+, Ca^{2+} and Mg^{2+} in ~~Lou soil~~Anthrosol and ~~cinnamon soil~~Calcisol colloidal suspensions decreased with the decreasing colloidal particle diameter (Table S3), which was mainly due to the dilution effect during the extraction process.

Furthermore, Table S3 showed that the soluble cation contents were rather low, and their effects on the CCCs of soil colloids could be neglected.

(*Insert Figure 4 near here*)

Based on Figs. 3 and 4, 3 mmol·L^{-1} $CaCl_2$ solution could cause fast aggregation of soil colloidal particles, while it required at least 80 mmol·L^{-1} NaCl solution for comparable aggregation rate, indicating that the shielding effect of divalent cations on negative charges of colloids was stronger than that of monovalent cations. The quantitative calculation results showed that the CCC ratios of monovalent ion and divalent ion system were between 25.64 and 27.09, which conformed to the Schulze-Hardy rule (Baalousha, 2017).

For each type of the soil colloids, the higher the absolute zeta potential values of colloidal particles, the more negative charges carried on the surface, and the higher the stability (CCCs) of suspension. For the same particle diameter, e.g. d < 100 nm, the absolute zeta potentials of ~~Lou soil~~Anthrosol colloids were larger (Fig. 2) while the corresponding CCC was lower (Figs. 3 and 4). Study on the stability of biochar nanoparticles showed that the absolute values of zeta potentials could not be used to directly explain the stability difference among biochar nanoparticles from different feedstock materials but could explain the influences of solution conditions on the stability of biochar nanoparticles derived from the same feedstock material (Xu et al., 2020a).

The CCCs of ~~Lou soil~~Anthrosol and ~~cinnamon soil~~Calcisol colloids increased with decreasing diameter; that is, the CCCs of ~~Lou soil~~Anthrosol and ~~cinnamon soil~~Calcisol

colloids both showed the size effects. Hsu and Kuo (1995) demonstrated that the CCCs would generally decrease with the increasing particle diameter because smaller particles possess thicker double electric layers and higher electrolyte concentration is needed to neutralize charges on the surface, which were consistent with the results of ~~Lou soil~~Anthrosol and ~~cinnamon soil~~Calcisol colloids. The above explanation by Hsu and Kuo (1995) was derived from homogenous particles whose composition does not change with particle diameter. The results of this paper show that, for those two alkaline soils being such heterogeneous materials, when the organic matter contents and mineral types changed with colloidal particle diameter, the CCCs in monovalent and divalent solutions also decreased with increasing particle diameter.

In this paper, the organic matter contents of soil nanoparticles were the highest, so the CCCs were the largest, which were 1.7 and 2.4 times of the corresponding colloidal particles of d < 2 μm. The suspension stability of different clay minerals has been reported to vary with the mineralogical structure. The CCC of illite (≈100 mM) in NaCl solution was significantly higher than that of kaolinite (≈20 mM) (Jiang et al., 2012; Xu et al., 2017), indicating that the stability of illite suspensions is significantly higher than that of kaolinite. So ~~A~~another possible reason for the higher stability of soil nanoparticles is the increase of illite content and the decrease of kaolinite content. Therefore, the differences in organic matter contents and clay mineralogy are the fundamental reasons for the differences in colloidal suspension stability behind the size effects of ~~Lou soil~~Anthrosol and ~~cinnamon soil~~Calcisol colloids.

4. Conclusion

This study obtained soil colloidal fractions with three different particle sizes from Anthrosol and Calcisol using high-speed centrifugation and revealed the particle size effects on the soil constitutes, surface properties, and aggregation behavior of heterogeneous soil colloids. The results showed that, compared to coarse colloids (d < 2 μm and d < 1 μm), the organic carbon contents of Anthrosol and Calcisol nanoparticles were higher, at 27.38 $g \cdot kg^{-1}$ and 28.31 $g \cdot kg^{-1}$, respectively, approximately twice and three times that of the coarse colloids and the bulk soils, indicating that nanoparticles exhibit a strong potential for carbon sequestration. The absolute zeta potential values of soil nanoparticles decreased with decreasing average particle diameter, indicating a reduction in charge density. Anthrosol and Calcisol nanoparticles exhibited greater suspension stability in NaCl and $CaCl_2$ solutions. On one hand, this was due to the increased thickness of the double electric layer on the surface of soil nanoparticles, resulting in stronger repulsive forces between particles; on the other hand, it was due to the presence of more illite, which has higher CCC compared to other clay minerals. In conclusion, for such a highly heterogeneous system as soil, the size effects on soil colloidal suspension stability are strongly influenced by variations driven by essentially mineral composition. Future studies should further explore the mechanisms underlying the size effects of the typical soils on particle interactions, coagulation, and transport behaviors under environmentally relevant conditions.

~~The size effect of heterogeneous soil colloidal particles was demonstrated. The number-weighted diameters for Lou soil and cinnamon soil colloids of d < 100 nm were~~

~~72.47 nm and 85.48 nm, respectively. With the decreasing colloidal particle diameter, the total carbon content, organic carbon, organic functional groups content and illite all increased, indicating the finer particle size of the organic faction and illite. The absolute zeta potential values and the charge variability decreased with the decreasing particle diameter. Aggregation rates of soil colloids decreased with the decreasing of particle diameter at the same electrolyte concentration, which was particularly evident in RLA stage. In NaCl or $CaCl_2$ solution, the CCCs increased with the decreasing Lou soil and cinnamon soil colloidal particle diameter, indicating that the suspension stability was enhanced. These findings have important implications for predicting the environmental behaviors of soil colloids and related colloid-facilitated nutrient/contaminant transport.~~

Acknowledgments

This work was supported by Natural Science Foundation of Shaanxi Province (2023-JC-YB-263) and the National Natural Science Foundation of China (41701261), and the Fundamental Research Funds for the Central Universities (2452020165).

Author Contributions

Conceptualization, Xu, C.Y., Geng, Z.C., and Hu, F.N.; methodology, Xu, C.Y.; software, Yan, Y.Y.; formal analysis, Liu, J.J.; investigation, Zhang, X.R.; resources, Yan, Y.Y.; writing—original draft, Yan, Y.Y.; writing—review and editing, Xu, C.Y., and Hu, F.N.; visualization, Xu, C.Y., and Yan, Y.Y.; funding acquisition, Xu, C.Y.,

Geng, Z.C. and Hu, F.N.. All authors have read and agreed to the published version of the manuscript.

Declaration of Interest Statement

The authors declare that they have no known competing financial interests or personal relationships that could have appeared to influence the work reported in this paper.

References

Audette, Y., Congreves, K.A., Schneider, K., Zaro, G.C., Nunes, A.L.P., Nunes, A.L.P., Zhang, H.J., Voroney, R.P.: The effect of agroecosystem management on the distribution of C functional groups in soil organic matter: A review. Biol. Fertil. Soils. 57, 881–894, 2021.

Baalousha, M.: Aggregation and disaggregation of iron oxide nanoparticles: Influence of particle concentration, pH and natural organic matter. Sci. Total Environ. 407(6), 2093–2101, 2009.

Baalousha, M.: Effect of nanomaterial and media physicochemical properties on nanomaterial aggregation kinetics. NanoImpact. 6, 55–68, 2017.

Cárdenas, J.P., Santiago, A., Tarquis, A.M., Losada, J.C., Borondo, F., Benito, R.M.: Soil porous system as heterogeneous complex network. Geoderma. 160(1), 13–21, 2010.

Chenu, C., Plante, A.F.: Clay-sized organo-mineral complexes in a cultivation

chronosequence: revisiting the concept of the‘primary organo-mineral complex’. Eur J Soil Sci. 57(4), 596–607, 2006.

Ding, W., Liang, H.X., Zhang, H.W., Sun, H., Geng, Z.C., Xu, C.Y.: A cellulose/bentonite grafted polyacrylic acid hydrogel for highly-efficient removal of Cd(II). J. Water Process. Eng. 51, 103414, 2023.

Dong, S.N., Zeng, Z., Cai, W.W., Zhou, Z.Y., Dou, C.B., Liu, H., Xia, J.H.: The zeta potentials of g-C_3N_4 nanoparticles: Effect of electrolyte, ionic strength, pH, and humic acid. J. Nanopart Res. 21, 233, 2019.

Filella, M., Zhang, J.W., Newman, M.E., Buffle, J.: Analytical applications of photon correlation spectroscopy for size distribution measurements of natural colloidal suspensions: capabilities and limitations. Colloid Surf. A. 120(1–3), 27–46, 1997.

He, Y.T., Wan, J., Tokunaga, T.: Kinetic stability of hematite nanoparticles, The effect of particle sizes. J. Nanopart Res. 10, 321–332, 2008.

Hou, J., Li, H., Zhu, H.L.,Wu, L.S.: Determination of clay surface potential, a more reliable approach. Soil Sci Soc Am J. 73(5), 1658–1663, 2009.

Hsu, J.P., Kuo, Y.C.: An Extension of the Schulze-Hardy Rule to Asymmetric Electrolytes. J. Colloid Interface Sci. 171(1), 254–255, 1995.

Hu, N., Xu, C.Y., Geng, Z.C., Hu, F.N., Li, Q.R., Ma, R.T., Wang, Q.: The interplay of particle properties and solution chemistry on aggregation kinetics of soil nanoparticles. J Soils Sediments. 22, 1761–1772, 2022.

IUSS Working Group WRB. World Reference Base for Soil Resources. International soil classification system for naming soils and creating legends for soil maps. 4th

edition. International Union of Soil Sciences (IUSS), Vienna, Austria. 2022.

Jiang, C.L., Séquaris, J.M., Vereecken, H., Klumpp, E.: Effects of inorganic and organic anions on the stability of illite and quartz soil colloids in Na-, Ca- and mixed Na-Ca systems. Colloids Surf. A. 415, 134–141, 2012.

Lead, J.R., Wilkinson, K.J.: Aquatic Colloids and Nanoparticles: Current Knowledge and Future Trends. Environ. Chem. 3(3), 159–171, 2006.

Li, S.X., Luo, Y.M., Zhang, H.B., Huang, Y.J., Li, Z., Wei, J.: Arsenic forms in various particle-size fractions of red soil-Chemical fractionation and speciation using XANES analysis. Acta Scientiae Circumstantiae. 31(12), 2733–2739, 2011.

Li, W. Y., Zhu, X.Y., He, Y., Xing, B. S., Xu, J.M.: Enhancement of water solubility and mobility of phenanthrene by natural soil nanoparticles. Environ Pollut. 176, 228–233, 2013.

Liang, H.X., Sun, R.R., Song, B., Sun, Q.Q., Peng, P., She, D.: Preparation of nitrogen-doped porous carbon material by a hydrothermal-activation two-step method and its high-efficiency adsorption of Cr(VI). J. Hazard. Mater. 387, 121987, 2020.

Luo, J.J., Niu, Q., Jin, M.C., Cao, Y.A., Ye, L.R., Du, R.P.: Study on the effects of oxygen-containing functional groups on Hg^0 adsorption in simulated flue gas by XAFS and XPS analysis. J. Hazard. Mater. 376(15), 21–28, 2019.

Mayordomo, N., Degueldre, C., Alonso, U., Missana, T.: Size distribution of FEBEX bentonite colloids upon fast disaggregation in low-ionic strength water. Clay Miner. 51(2), 213–222, 2016.

574 Meng, Z.Y., Hashmi, S.M., Elimelech, M.: Aggregation rate and fractal dimension of
575 fullerene nanoparticles via simultaneous multiangle static and dynamic light
576 scattering measurement. J. Colloid Interface Sci. 392, 27–33, 2013.
577 Moayedi, H., Kazemian, S.: Zeta potentials of suspended humus in multivalent cationic
578 saline solution and its effect on electro-osomosis behavior. J. Dispers Sci. Technol.
579 34(2), 283–294, 2013.
580 Said-Pullicino, D., Giannetta, B., Demeglio, B., Missong, A., Gottselig, N., Romani,
581 M., Bol, R., Klumpp, E., Celi, L.: Redox-driven changes in water-dispersible
582 colloids and their role in carbon cycling in hydromorphic soils. Geoderma. 385,
583 114894, 2021.
584 Schäfer, T., Huber, F., Seher, H., Missana, T., Alonso, U., Kumke, M., Eidner, S., Claret,
585 F., Enzmann, F.: Nanoparticles and their influence on radionuclide mobility in
586 deep geological formations. Appl. Geochemistry. 27(2), 390–403, 2012.
587 Song, B.Q., Chen, M., Zhao, L., Qiu, H., Cao, X.D.: Physicochemical property and
588 colloidal stability of micron- and nano-particle biochar derived from a variety of
589 feedstock sources. Sci. Total Environ. 661, 685–695, 2019.
590 Sun, Y.L., Pan, D.Q., Wei, X.Y., Xian, D.F., Wang, P., Hou, J.J.: Insight into the stability
591 and correlated transport of kaolinite colloid: Effect of pH, electrolytes and humic
592 substances. Environ. Pollut. 266, 115189, 2020.
593 Tan, Z.X., Yuan, S.N., Hong, M.F., Zhang, L.M., Huang, Q.Y.: Mechanism of negative
594 surface charge formation on biochar and its effect on the fixation of soil Cd. J.
595 Hazard. Mater. 384, 121370, 2019.

596 Tang, Y., Li, H., Liu, X.M., Zhu, H.L., Tian, R.: Unraveling the size distributions of
597 surface properties for purple soil and yellow soil. J Environ Sci (China). 32, 81–
598 89, 2015.
599 Tsao, T.M., Chen, Y.M., Sheu, H., Tzou, Y.M., Chou, Y.M., Wang, M.K.: Separation
600 and identification of soil nanoparticles by conventional and synchrotron X-ray
601 diffraction. Appl. Clay Sci. 85, 1–7, 2013.
602 Tsao, T.M., Chen, Y.M., Wang, M.K., Huang, P.M.: Structural transformation and
603 physicochemical properties of environmental nanoparticles by comparison of
604 various particle-size fractions. Soil Sci Soc Am J. 75(2), 533–541, 2011.
605 Wang, L.F., Wang, L.L., Ye, X.D., Li, W.W., Ren, X.M., Sheng, G.P., et al.: Coagulation
606 kinetics of humic aggregates in mono-and divalent electrolyte solutions. Environ.
607 Sci. Technol. 47(10), 5042–5049, 2013.
608 Wang, Q.R., Li, Y.C., Wang, Y.: Optimizing the weight loss-on-ignition methodology
609 to quantify organic and carbonate carbon of sediments from diverse sources.
610 Environ. Monit. Assess. 174, 241–257, 2011.
611 Wei, X.Y., Pan, D.Q., Xu, Z., Xian, D.F., Li, X.L., Tan, Z.Y., Liu, C.L., Wu, W.S.:
612 Colloidal stability and correlated migration of illite in the aquatic environment:
613 The roles of pH, temperature, multiple cations and humic acid. Sci. Total Environ.
614 768, 144174, 2021.
615 Weil, R.R., Brady, N.C.: The Nature and Properties of Soils, Global Edition. Pearson
616 Education Limited. 2016.
617 Weissenberger, G., Henderikx, R.J., Peters, P.J.: Understanding the invisible hands of

618 sample preparation for cryo-EM. Nat. Methods. 18(5), 463–471, 2021.
619 Wilson, M. A., Tran, N. H., Milev, A. S., Kannangara, G. S. K., Volk, H.: Nanomaterials
620 in soils. Geoderma. 146, 291–302, 2008.
621 Won, J., Burns, S.E.: Role of Immobile Kaolinite Colloids in the Transport of Heavy
622 Metals. Environ. Sci. Technol. 52(5): 2735–2741, 2018.
623 Xu, C.Y., Deng, K.Y., Li, J.Y., Xu, R.K.: Impact of environmental conditions on
624 aggregation kinetics of hematite and goethite nanoparticles. J. Nanopart Res. 17,
625 394, 2015.
626 Xu, C.Y., Li, Q.R., Geng, Z.C., Hu, F.N., Zhao, S.W.: Surface properties and suspension
627 stability of low–temperature pyrolyzed biochar nanoparticles: Effects of solution
628 chemistry and feedstock sources. Chemosphere. 259, 127510, 2020a.
629 Xu, C.Y., Xu, R.K., Li, J.Y., Deng, K.Y.: Phosphate-induced aggregation kinetics of
630 hematite and goethite nanoparticles. J. Soils Sediments. 17, 352–363, 2017.
631 Xu, C.Y., Zhou, T.T., Wang, C.L., Liu, H.Y., Zhang, C.T., Hu, F.N., Zhao, S.W., Geng,
632 Z.C.: Aggregation of polydisperse soil colloidal particles: Dependence of
633 Hamaker constant on particle size. Geoderma. 359, 113999, 2020b.
634 Xu, Z., Pan, D.Q., Sun, Y.L., Wu, W.S.: Stability of GMZ bentonite colloids:
635 Aggregation kinetic and reversibility study. Appl. Clay Sci. 161, 436–443. 2018.
636 Yin, X.Q., Gao, B., Ma, L.Q., Saha, U.K., Sun, H.M., Wang, G.D.: Colloid-facilitated
637 Pb transport in two shooting-range soils in Florida. J. Hazard. Mater. 177(1–3),
638 620–625, 2010.
639 Yu, X., Fu, Y., Lu, S.: Characterization of the pore structure and cementing substances

of soil aggregates by a combination of synchrotron radiation X-ray micro–computed tomography and scanning electron microscopy. Eur. J. Soil Sci. 68(1), 66–79, 2017.

Zhang, Q., Bol, R., Amelung, W., Missong, A., Siemens, J., Mülder, I.: Water dispersible colloids and related nutrient availability in Amazonian Terra Preta soils. Geoderma. 397, 115103, 2021.

Zhang, Z.Y., Huang, L., Liu, F., Wang, M.K., Fu, Q.L., Zhu, J.: Characteristics of clay minerals in soil particles of two Alfisols in China. Appl. Clay Sci. 120, 51–60, 2016.

Zhou, D.X., Ji, Z.X., Jiang, X.M., Dunphy, D.R., Brinker, J., Keller A.A.: Influence of material properties on TiO_2 nanoparticle agglomeration. PLoS One. 8(11), e81239, 2013.

Zhu, X., Chen, H., Li, W., He, Y., Brookes, P.C., Xu, J.: Aggregation kinetics of natural soil nanoparticles in different electrolytes. Eur. J. Soil Sci. 65(2), 206–217, 2014.

Table captions

Table 1 The average diameters and distribution patterns of ~~Lou soil~~soil ~~and cinnamon soil~~ colloids.

Table 2 The physiochemical properties of ~~Lou soil~~soil ~~and cinnamon soil~~ colloids.

Table 3 The dominant clay minerals of ~~Lou soil~~ soil ~~and cinnamon soil~~ colloidal fractions (shown in mass fraction, %).

Table 4 The aggregation rates of ~~Lou soil~~soil ~~and cinnamon soil~~ colloids.

Table 1 The average diameters and distribution patterns of ~~Lou soil~~soil ~~and cinnamon soil~~ colloids

Soil ~~colloids~~type	Colloidal fractions	Number-weighted diameter (nm)	Intensity-weighted diameter (nm)	D_{10} (nm)	D_{90} (nm)
~~Lou soil~~Anthrosol ~~colloids~~	d < 2 μm	133.16 ± 24.28	396.81 ± 12.34	71.53	232.49
	d < 1 μm	127.84 ± 20.29	371.45 ± 11.88	67.64	219.87
	d < 100 nm	72.47 ± 7.04	294.10 ± 15.80	38.74	136.72
~~cinnamon soil~~Calcisol ~~colloids~~	d < 2 μm	141.23 ± 24.33	439.20 ± 12.72	78.29	244.97
	d < 1 μm	131.67 ± 15.77	372.07 ± 8.23	75.84	231.64
	d < 100 nm	85.48 ± 16.93	312.25 ± 33.58	47.84	158.99

Note: D_{10}, D_{50} and D_{90} represent diameter of particles with a cumulative distribution of 10%, 50% and 90%, respectively.

Table 2 The physiochemical properties of ~~Lou soil~~soil ~~and cinnamon soil~~ colloids

Soil ~~colloids~~type	Colloidal fractions	Yield (%)	Total carbon content ($g \cdot kg^{-1}$)	Organic carbon content ($g \cdot kg^{-1}$)	$CaCO_3$ content ($g \cdot kg^{-1}$)	Specific surface area ($m^2 \cdot g^{-1}$)
~~Lou soil~~Anthrosol ~~colloids~~	d < 2 μm	25.12	20.90 ± 0.30	10.90 ± 1.29	10.00	65.37
	d < 1 μm	18.76	20.65~~7~~ ± 0.15	10.91 ± 0.43	9.74~~8~~	72.99
	d < 100 nm	6.32	58.25 ± 0.35	27.~~4~~38 ± 0.21	30.87	45.28
~~cinnamon soil~~Calcisol ~~colloids~~	d < 2 μm	23.17	24.00 ± 0.30	11.~~7~~66 ± 0.60	12.34	49.99
	d < 1 μm	16.20	22.30 ± 0.20	12.~~8~~76 ± 0.11	9.54	61.88
	d < 100 nm	4.70	76.30 ± 0.40	28.31 ± 0.15	~~48.0~~47.99	34.53

671 **Table 3** The dominant clay minerals of ~~Lou soil~~soil ~~and cinnamon soil~~ colloidal fractions
672 (shown in mass fraction, %)

Soil ~~colloids~~type	Colloidal fractions	Illite	Kaolinite	Chlorite	Vermiculite
~~Lou soil~~Anthrosol ~~colloids~~	$d < 2$ μm	34	23	4	9
	$d < 1$ μm	30	22	7	11
	$d < 100$ nm	37	14	16	3
~~Cinnamon soil~~Calcisol ~~colloids~~	$d < 2$ μm	24	22	29	16
	$d < 1$ μm	31	19	25	12
	$d < 100$ nm	37	16	17	5

673

674 **Table 4** The aggregation rates of soil ~~Lou soil and cinnamon soil~~ colloids

Soil ~~colloids~~type	Colloidal fractions	Aggregation rate		Fractal dimension	
		In 50 mmol·L^{-1} NaCl (nm·min^{-1})	In 1 mmol·L^{-1} $CaCl_2$ (nm·min^{-1})	Na	Ca
~~Lou soil~~Anthrosol ~~colloids~~	d < 2 μm	19.46	12.01	1.69 ± 0.19	1.33 ± 0.26
	d < 1 μm	14.91	11.48	1.75 ± 0.06	1.52 ± 0.19
	d < 100 nm	7.72	9.97	1.71 ± 0.26	1.68 ± 0.13
~~Cinnamon soil~~Calcisol ~~colloids~~	d < 2 μm	8.98	8.22	1.30 ± 0.17	1.36 ± 0.17
	d < 1 μm	7.15	7.33	1.71 ± 0.24	1.30 ± 0.31
	d < 100 nm	3.95	5.22	1.52 ± 0.22	1.58 ± 0.19

675

Figure captions

Fig. 1. The photoelectron spectrum C1s and O1s peak diagram of ~~Lou soil~~Anthrosol and ~~cinnamon soil~~Calcisol colloids. C1s of ~~Lou soil~~Anthrosol colloids, a. $d < 2$ μm, b. $d < 1$ μm, c. $d < 100$ nm; C1s of ~~cinnamon soil~~Calcisol colloids, d. $d < 2$ μm, e. $d < 1$ μm, f. $d < 100$ nm; O1s of ~~Lou soil~~Anthrosol colloids, g. $d < 2$ μm, h. $d < 1$ μm, i. $d < 100$ nm; O1s of ~~cinnamon soil~~Calcisol colloids, j. $d < 2$ μm, k. $d < 1$ μm, l. $d < 100$ nm.

Fig. 2. The zeta potential of ~~Lou soil~~Anthrosol (a) and ~~cinnamon soil~~Calcisol (b) colloids of $d < 2$ μm, < 1 μm, and < 100 nm at different pH

Fig. 3. The CCCs of ~~Lou soil~~Anthrosol (a) and ~~cinnamon soil~~Calcisol (b) colloids of $d < 2$ μm, < 1 μm, and < 100 nm in NaCl solution

Fig. 4. The CCC of ~~Lou soil~~Anthrosol (a) and ~~cinnamon soil~~Calcisol (b) colloids of $d < 2$ μm, < 1 μm, and < 100 nm in CaCl2 solution

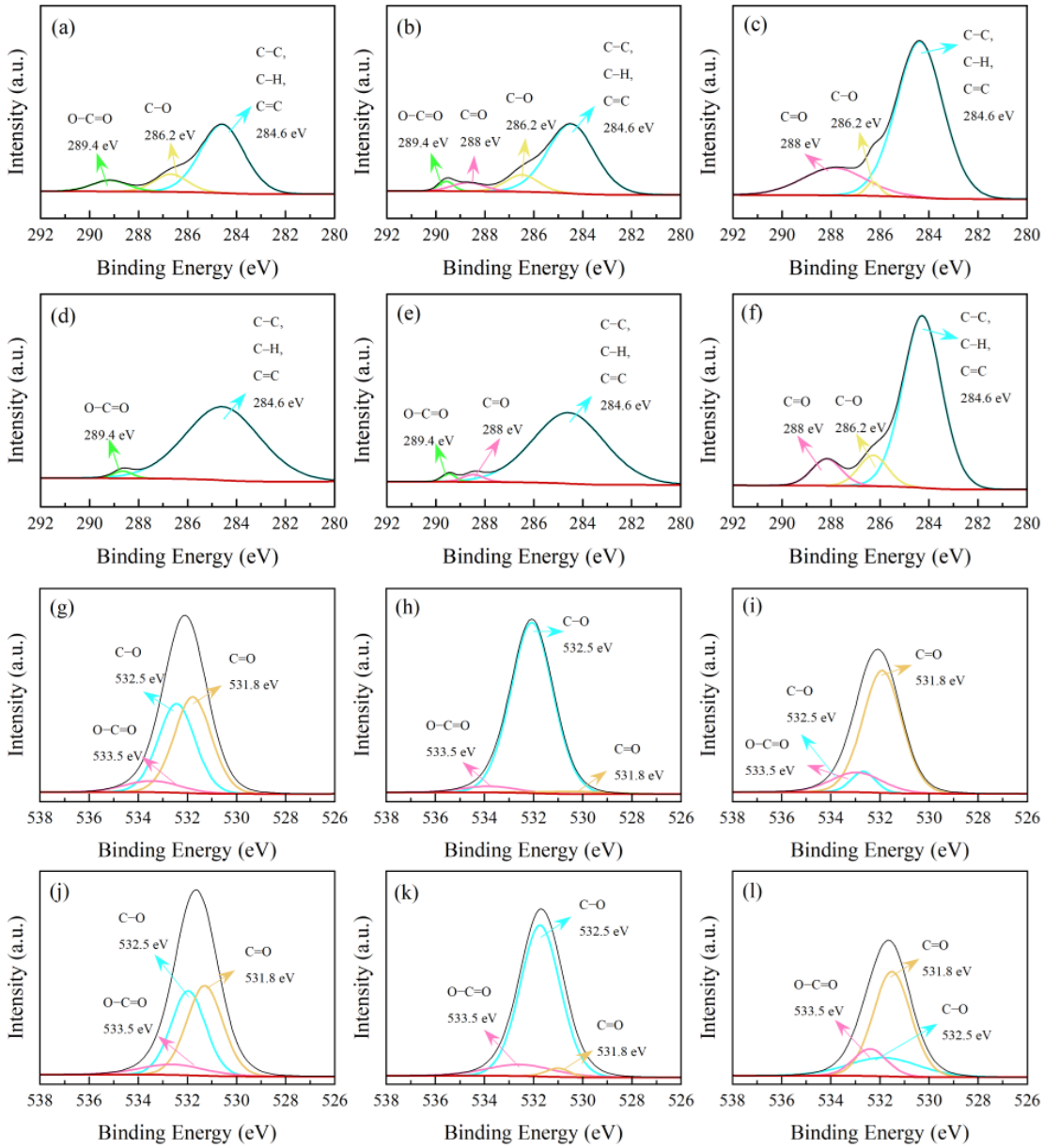

Fig. 1 The photoelectron spectrum C1s and O1s peak diagram of ~~Lou soil~~Anthrosol and ~~cinnamon soil~~Calcisol colloids. C1s of ~~Lou soil~~Anthrosol colloids, (a). $d < 2$ μm, (b). $d < 1$ μm, (c). $d < 100$ nm; C1s of ~~cinnamon soil~~Calcisol colloids, (d). $d < 2$ μm, (e). $d < 1$ μm, (f). $d < 100$ nm; O1s of ~~Lou soil~~Anthrosol colloids, (g). $d < 2$ μm, (h). $d < 1$ μm, (i). $d < 100$ nm; O1s of ~~cinnamon soil~~Calcisol colloids, (j). $d < 2$ μm, (k). $d < 1$ μm, (l). $d < 100$ nm.

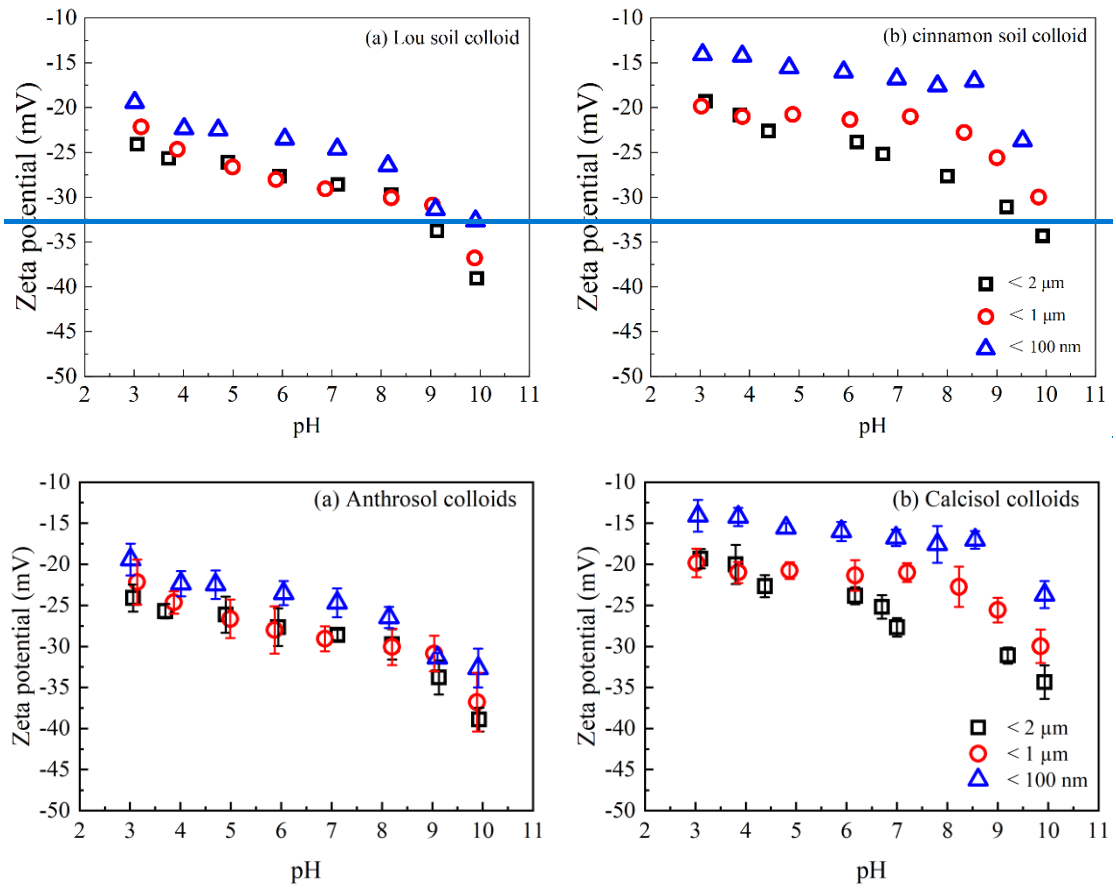

Fig. 2 The zeta potential of ~~Lou soil~~Anthrosol (a) and ~~cinnamon soil~~Calcisol (b) colloids of *d* < 2 μm, < 1 μm, and < 100 nm at different pH

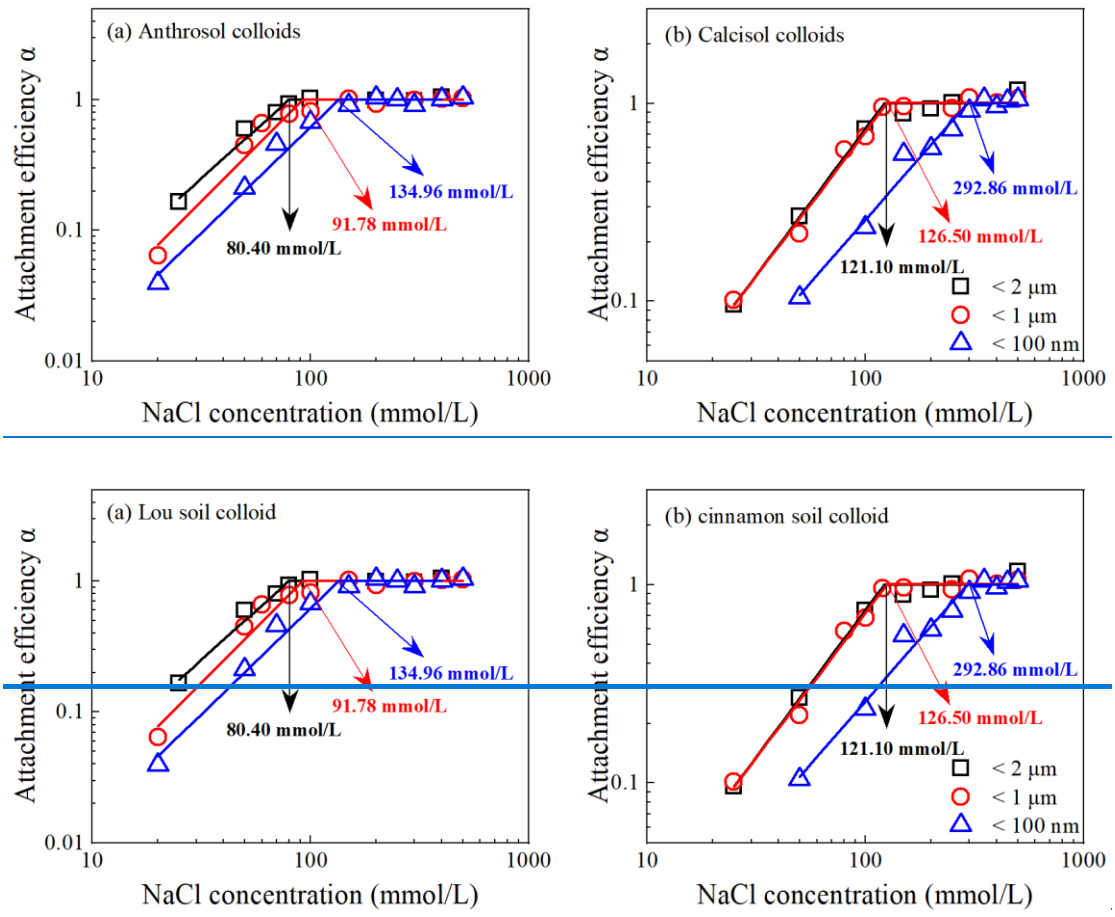

Fig. 3 The CCCs of ~~Lou soil~~Anthrosol (a) and ~~cinnamon soil~~Calcisol (b) colloids of $d < 2$ μm, < 1 μm, and < 100 nm in NaCl solution

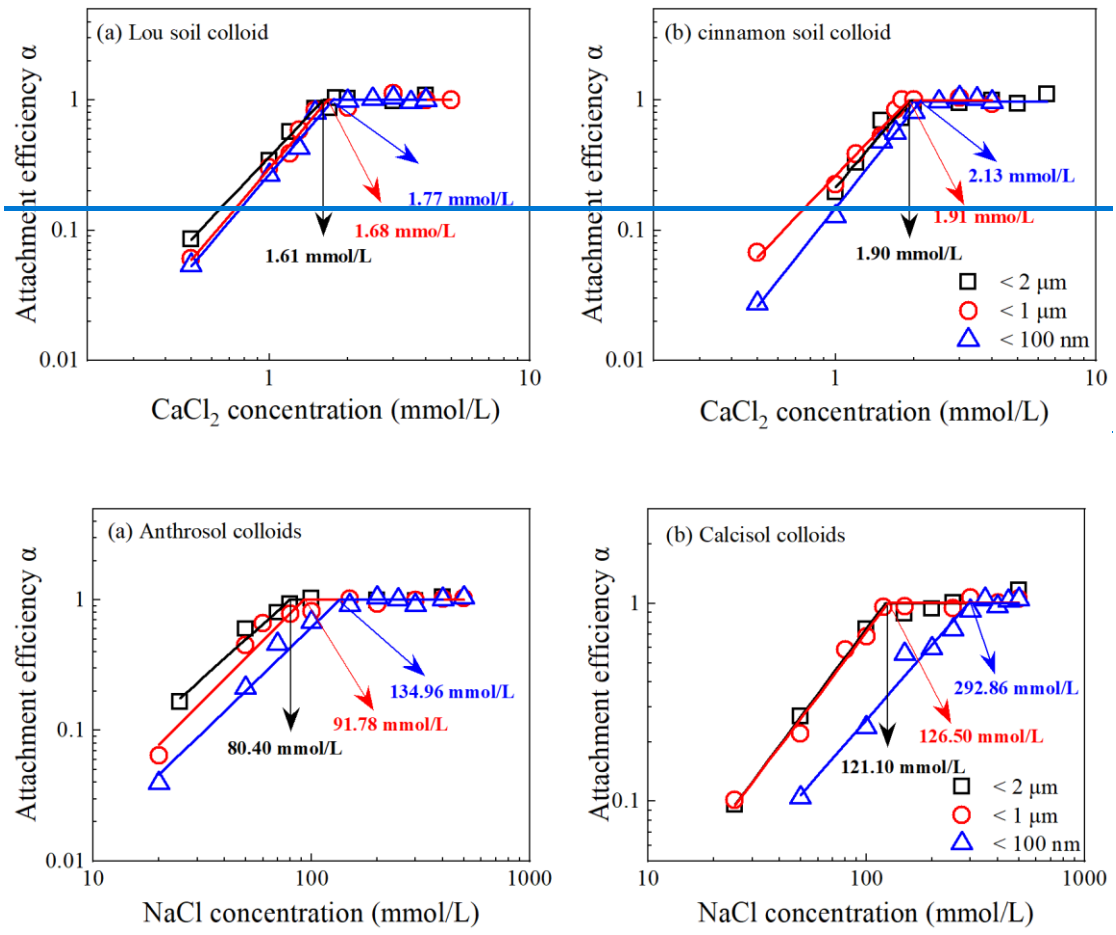

706

707

708 **Fig. 4** The CCC of ~~Lou soil~~Anthrosol (a) and ~~cinnamon soil~~Calcisol (b) colloids of $d < 2$ μm,

709 < 1 μm, and < 100 nm in $CaCl_2$ solution。